Q. J. R. Meteorol. Soc. (2006), **132**, pp. 1–17 doi: 10.1256/qj.05.70

Understanding the variability of clear-sky outgoing long-wave radiation based on ship-based temperature and water vapour measurements

By V. O. JOHN[1,2]*, S. A. BUEHLER[1,3], A. von ENGELN[4], P. ERIKSSON[5], T. KUHN[6], E. BROCARD[7] and G. KOENIG-LANGLO[8]

[1]*Institute of Environmental Physics, University of Bremen, Germany*
[2]*Rosenstiel School of Marine and Atmospheric Science, University of Miami, USA*
[3]*Department of Space Science, Lulea Technical University, Kiruna, Sweden*
[4]*EUMETSAT, Darmstadt, Germany*
[5]*Radio and Space Science, Chalmers University of Technology, Gothenburg, Sweden*
[6]*I. Physikalisches Institut, University of Cologne, Germany*
[7]*Institute of Applied Physics, University of Bern, Switzerland*
[8]*Alfred Wegener Institute for Polar and Marine Research, Bremerhaven, Germany*

(Received 22 April 2005; revised 27 July 2006)

SUMMARY

High-resolution radiative transfer model calculations with the Atmospheric Radiative Transfer Simulator (ARTS) were used to simulate the clear-sky outgoing long-wave radiative flux (OLR) at the top of the atmosphere. The unique set of radiosonde data collected by the research vessel *Polarstern* of the Alfred Wegener Institute for Polar and Marine Research during 27 expeditions in the years 1982 to 2003 was used to investigate the sources of clear-sky OLR variability for ocean areas in different climate zones and seasons. For this dataset, tropospheric temperature variations contribute approximately 33 W m^{-2} OLR variability, tropospheric relative humidity variations 8.5 W m^{-2}, and vertical structure 2.3–3.4 W m^{-2}. Of these, 0.3–1.0 W m^{-2} are due to structures on a vertical scale smaller than 4 km, which cannot be resolved by conventional remote-sensing instruments. It was also found that the poor absolute accuracy of current humidity data in the upper troposphere, approximately 40% relative error in relative humidity, leads to a significant uncertainty in OLR of about 3.8 W m^{-2} (for a midlatitude summer atmosphere), which should be put in the context of the double CO_2 effect of only 2.6 W m^{-2} (for the same atmosphere).

KEYWORDS: Humidity Vertical structure

1. INTRODUCTION

The planet Earth is in radiative equilibrium with its surroundings. It receives energy in the form of short-wave radiation from the sun and loses energy in the form of long-wave radiation to space. These two radiation streams can be represented approximately by blackbody radiation of 6000 K for the solar short-wave radiation and 290 K for the terrestrial long-wave radiation. The balance between the incoming short-wave radiation and the outgoing long-wave radiation (OLR) determines the temperature in the atmosphere and on the Earth's surface (Salby 1996; Harries 1996, 1997).

The OLR originates partly from the surface and partly from higher levels of the atmosphere. Because of the lower temperature of these levels compared to the surface, the OLR is reduced compared to a hypothetical Earth without atmosphere. This is the atmospheric 'greenhouse' effect. From the known incoming solar short-wave radiation we can easily infer the global average OLR to be close to 240 W m^{-2} because the incoming and outgoing radiation fluxes must balance (Harries 1996). However, there is considerable variability for different latitudes and weather conditions, so that local OLR values vary between about 160 W m^{-2} and 320 W m^{-2}. Allan *et al.* (1999) showed that the clear-sky OLR variability is mostly due to temperature variability at high latitude and mostly due to humidity variability at low latitude.

* Corresponding author: Rosenstiel School of Marine and Atmospheric Science, University of Miami, Miami, FL 33149, USA. e-mail: vojohn@rsmas.miami.edu

Clough *et al.* (1992) and Clough and Iacono (1995) showed that water vapour has a significant effect on OLR not only in the pure rotational band from approximately 0 to 600 cm^{-1} and the vibrational-rotational band from approximately 1400 to 2100 cm^{-1}, but also in the continuum region between the bands. Moreover, these different frequency regions of water vapour absorption are responsible for OLR sensitivity to water vapour perturbations at different altitudes, a fact first pointed out by Sinha and Harries (1995), who particularly stressed the importance of the 0 to 500 cm^{-1} frequency region, where OLR is sensitive to perturbations in the middle and upper troposphere.

The considerable interest in the sensitivity of OLR to humidity variations at different altitudes is mainly due to the debate about the humidity feedback in the climate system that was started by Lindzen (1990). A very good overview of this debate is given by Held and Soden (2000). The broad consensus now seems to be that the feedback is indeed positive, not negative as conjectured by Lindzen (see, for example, Shine and Sinha 1991; Sinha and Allen 1994; Colman 2001). However, the exact magnitude of the feedback is still somewhat uncertain, not least because of our insufficient knowledge of the absolute amount of upper-tropospheric humidity, due to the limitations of the current global observing system. For example, there are large differences between the humidity measured by radiosondes and by infrared sensors as documented by Soden and Lanzante (1996) and Soden *et al.* (2004). Another limitation is that typical atmospheric humidity profiles are rich in vertical structure, as documented by radiosondes, while current remote-sensing methods usually yield only vertically smoothed measurements with a smoothing height of 2.5 to 6.0 km, depending on the technique.

The present study had the objective to understand the global variability of clear-sky OLR and its dependence on variations in atmospheric temperature and humidity. This is achieved by using the unique radiosonde record collected during the voyages of the research vessel *Polarstern* as input to high-resolution radiative transfer model calculations. The dataset is limited to the ocean areas, and thus does not provide true global coverage. However, because of the long cruises of *Polarstern* from pole to pole, the dataset has a significantly better continuous latitude coverage of both hemispheres than any other radiosonde dataset known to the authors.

An additional objective of the study was to assess the impact of vertical structure in the humidity field on OLR, and to assess to what extent humidity measurements with coarse vertical resolution can be used to predict OLR. As a caveat to these study objectives, it has to be pointed out that understanding the spatial variability of OLR is not sufficient to predict its response to a large-scale forcing, such as a CO_2 increase. A better strategy for that application is to look at the impact of other large-scale forcings, for example a large volcano eruption, as done by Soden *et al.* (2002). However, understanding this variability can give important insights on the relevant factors controlling OLR and can help identify deficiencies in our observational capabilities.

Clouds also have an important impact on OLR, but this study focuses only on the clear-sky case. Clouds reduce OLR in the same manner as other greenhouse gases and the magnitude of this impact depends on the cloud altitude. On average the cloud effect on OLR is 30 W m^{-2} (Kiehl and Trenberth 1997). It should be noted that clear-sky OLR here means that the radiances were calculated without considering the effects of clouds on the radiation, but the profile used for calculating the radiances might have sampled cloudy atmospheres whereas clear-sky OLR estimated from satellite data samples only atmospheres without clouds. This can result in a higher OLR for satellite-based datasets and a lower OLR for the type of calculations used in this study or other previous studies of this type (Slingo *et al.* 1998; Allan *et al.* 1999).

The paper is organized as follows: section 2 presents the radiative transfer model and the atmospheric dataset, section 3 results and discussion, and section 4 summary and conclusions.

2. Model set-up and atmospheric profiles

(*a*) *Radiative transfer model*

Detailed line-by-line radiative transfer calculations were performed with the Atmospheric Radiative Transfer Simulator (ARTS), described in Buehler *et al.* (2005). The model assumes a realistic spherical geometry for the atmosphere, which is an important difference from older models that assume a plane-parallel atmosphere. The model was used to simulate the OLR, defined here as the upwelling radiative flux at 100 Pa. The reference altitude of 100 hPa was chosen because of the limited coverage of higher altitudes in radiosonde data (see section 2(b)). How to set the model up for OLR calculations is described in detail in Buehler *et al.* (2006), hereafter referred to as BEB. BEB also gives such theoretical background as the formal definition of radiative fluxes and OLR. We will therefore not repeat this information here.

The considered spectral range is from 0 to 2500 cm^{-1}, similar to Clough and Iacono (1995). The most important radiatively active species in this spectral region are water vapour, carbon dioxide, methane, nitrous oxide and ozone, with water vapour being by far the most important one. The calculation was therefore limited to these five key species in order to reduce the computational burden. The spectral line database for the calculations was HITRAN*-2000 (Rothman *et al.* 2003). In addition to the line spectra, various continua have to be taken into account. As in BEB, continuum parametrizations were taken from Clough *et al.* (2005). The surface emissivity was set to unity, following Clough *et al.* (1992). Although the sea surface emissivity varies slightly with sea surface temperature and salinity (Newman *et al.* 2005), the approximation of sea surface emissivity to unity is good enough at infrared frequencies. The top of the atmosphere was assumed to be at 100 hPa unless otherwise stated.

A sensitivity study was performed using profiles from the European Centre for Medium-range Weather Forecasts (ECMWF) to check the impact of the levels above 100 hPa on OLR. The profiles used are the reduced dataset (80 profiles) described in Chevallier (2001). The results show that the OLR at 100 hPa ($\sim$15 km) and at the top of the atmosphere (60 km) are highly correlated (0.998). The difference in standard deviation between these two sets of OLR data is only 0.6 W m^{-2}. We used temperature, humidity, and ozone profiles from the dataset and for nitrous oxide, methane, and carbon monoxide, FASCOD† (Anderson *et al.* 1986) climatological profiles were used. On average, the 100 hPa OLR value is 6.4 W m^{-2} higher than that at the top of the atmosphere (60 km).

The model set-up was exactly as described in BEB, with the following exceptions. Firstly, the species list contained only the five main species as mentioned above. The impact of this species reduction is that the OLR can be increased by approximately 0.1%. Secondly, a frequency grid of 10 000 points uniformly spaced between 0 and 2500 cm^{-1} was used for all calculations, except the ones dealing with vertical structure. For the vertical structure simulations, a reduced frequency grid with only 1000 uniformly spaced points was used. The bias introduced by the reduced grid is below

* HIgh-resolution TRANsmission molecular absorption database.

† Fast Atmospheric Signature CODe.

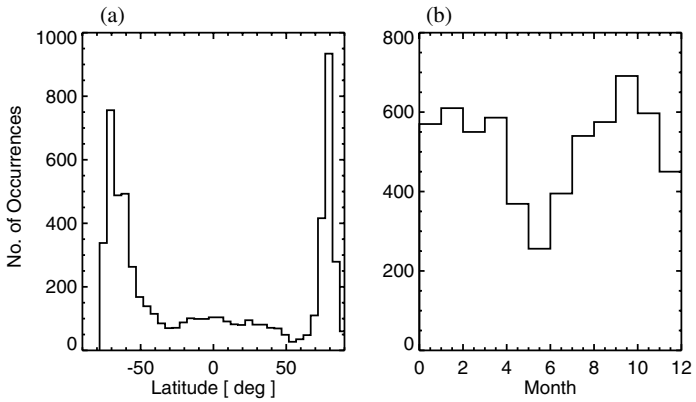

Figure 1. (a) Latitudinal and (b) temporal coverage of the *Polarstern* radiosonde data. For seasonal coverage, see Table 1.

TABLE 1. DEFINITION OF RADIOSONDE CLASSES AND NUMBER OF PROFILES IN EACH CLASS

	Latitude range (°)		Month range		
Class	NH	SH	NH	SH	No. of profiles
TRO	0–20	−20 to 0	5–9	5–9	150
MLS	35–50	−35 to −50	6–8	12–2	139
MLW	35–50	−35 to −50	12–2	6–8	52
SAS	55–75	−55 to −75	6–8	12–2	1279
SAW	55–75	−55 to −75	12–2	6–8	69

NH, SH = northern, southern hemisphere. See text for class acronyms.

approximately 0.3% or 1 W m^{-2}. Both changes were made to reduce the computational burden, but have no impact on the study conclusions.

(*b*) *Atmospheric profiles*

For a model study of the variability of OLR, one needs an atmospheric dataset that captures the variability in the atmospheric state, most importantly in the profiles of temperature and humidity. Earlier studies have used data from a general-circulation model (Allan *et al.* 1999), but one can also use direct measurements of humidity and temperature. If one wants to study the impact of vertical structure, the only available dataset with high enough vertical resolution is radiosonde data. However, the synoptic radiosonde station network has very uneven latitudinal coverage, particularly in the tropics and over the entire southern hemisphere.

Therefore, this study uses the unique set of radiosonde data collected by the research vessel *Polarstern* of the Alfred Wegener Institute for Polar and Marine Research (AWI) during 27 expeditions in the years 1982 to 2003 (Koenig-Langlo and Marx 1997). The dataset comprises 6189 individual profiles. It has a fairly good latitudinal and seasonal coverage, as demonstrated by Fig. 1, although high latitudes and the summer season are over-represented (see Table 1). The data allow the generation of five different classes, corresponding to seasons and latitude ranges: tropical (TRO), midlatitude summer (MLS), midlatitude winter (MLW), subarctic summer (SAS), and subarctic winter (SAW). Table 1 gives the definitions of these classes and the number of profiles

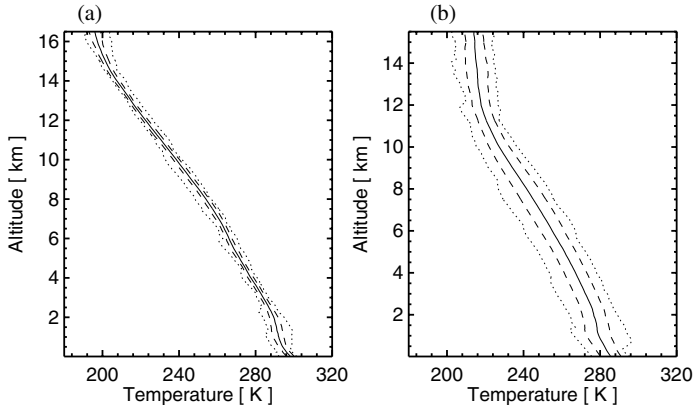

Figure 2. Temperature statistics for (a) the TRO class and (b) the MLS class: mean profile (solid), the mean ± one standard deviation (dashed), and the maximum/minimum (dotted).

in each class. Note that the number of profiles in each class varies from over 1200 for SAS to about 50 for MLW.

To have an equal number of profiles for each class, 50 profiles for each class were randomly selected. Figure 2 shows the temperature statistics for the TRO and MLS classes. As expected from re-analysis data, the variability for the TRO class is much lower than the variability for the MLS class (von Engeln *et al.* 2004). Figure 3 shows the humidity statistics for the same two classes, showing that, in spite of the more homogeneous temperature in the tropics, humidity variability is as high as at midlatitudes. This is true for both absolute and relative humidity.

The profiles normally reached up to an altitude of 18–30 km. As each profile reached a different altitude, all the profiles were cut at 100 hPa. This corresponds to an altitude of approximately 16.5 km for the TRO class, 15.5 km for the MLS and MLW classes, 15.0 km for the SAS class, and 14.5 km for the SAW class. This is above the tropopause, except for a few cases in the TRO scenario (average tropopause height for the tropical class, calculated using all the *Polarstern* radiosonde profiles, is 16.9 km whereas the average 100 hPa height is 16.6 km). Since the radiosonde data contain only temperature and humidity information, concentrations of CO_2, O_3, N_2O, and CH_4 were taken from the corresponding FASCOD scenarios (Anderson *et al.* 1986).

To investigate the role of fine vertical structures in the humidity profiles, various smoothed profiles were generated taking running means of the high-resolution profiles over a certain altitude range (boxcar smoothing). The smoothing heights applied were 500 m, 1000 m, 2000 m, and 4000 m. The larger the smoothing height, the more the vertical structure is lost, as demonstrated by Fig. 4. It is crucial to note that the result of the smoothing strongly depends on the humidity unit. Figure 5 shows how large the differences are between smoothing in volume mixing ratio (VMR), smoothing in log(VMR), and smoothing in relative humidity (RH). Smoothing in VMR increases the total column water vapour (TWV), while smoothing in log(VMR) reduces TWV. Smoothing in RH can produce either effect, depending on the profile. Two additional options investigated were smoothing in RH or VMR, but rescaling the smoothed profile so that TWV is conserved (called RH_c and VMR_c smoothing).

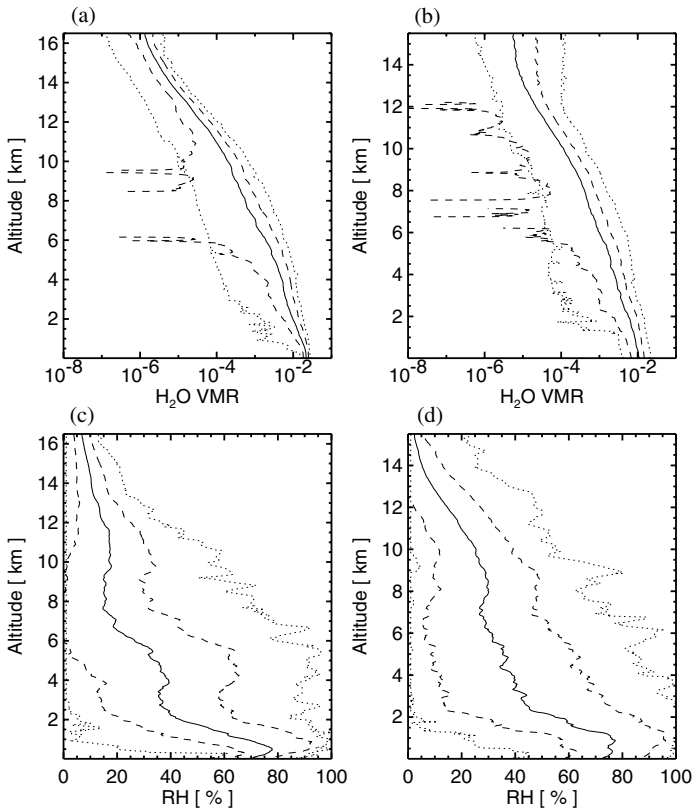

Figure 3. Volume mixing ratio (VMR, kg kg^{-1}) statistics for (a) the TRO class and (b) the MLS class: mean (solid), mean $\pm$ one standard deviation (dashed), and maximum/minimum (dotted). (c) and (d) are as (a) and (b), but for relative humidity (RH). The VMR profiles are plotted on a logarithmic scale, which explains the breaks in the mean minus one standard deviation curve when the standard deviation is greater than the mean value at certain altitudes.

3. Results and discussion

(*a*) *Mean and variability of clear-sky OLR*

Figure 6 shows the mean, $\overline{\mathrm{OLR}}$, and standard deviation, σ_{OLR}, of the OLR at 100 hPa for the different radiosonde classes. Extreme values are also indicated, and exact numbers are given in Table 2. The σ_{OLR} is close to 10 Wm^{-2}, except for the SAW case where it is significantly higher. Compared to the OLR values for the FASCOD climatological scenarios, which are given in BEB, the radiosonde values are significantly different, especially for the MLW and SAS scenarios. This is mostly because the FASCOD scenarios are not representative for these cases (von Engeln *et al.* 2004). A calculation with climatological profiles derived from ECMWF analysis data (not shown) yielded a better agreement. With similar latitude and time bins as for the radiosonde data, the ECMWF data OLR values were within one standard deviation of the radiosonde OLR values for the MLS, SAS, and SAW classes, and within 2 standard deviations of the radiosonde OLR values for the TRO and MLW classes. We consider this a satisfactory agreement, because the radiosonde sample is not large enough to exactly reproduce the climatological mean values, especially in the MLW case.

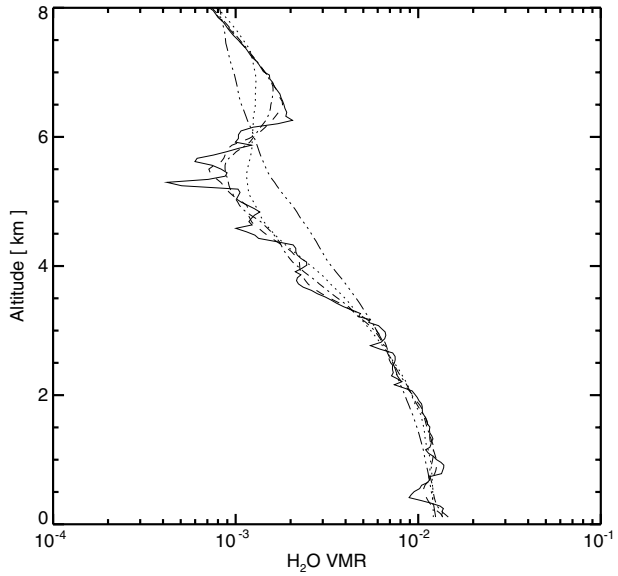

Figure 4. A typical original radiosonde VMR profile (solid), and smoothed profiles (VMR smoothing) with smoothing heights 500 m (dashed), 1000 m (dash-dotted), 2000 m (dotted), and 4000 m (dash-triple-dotted).

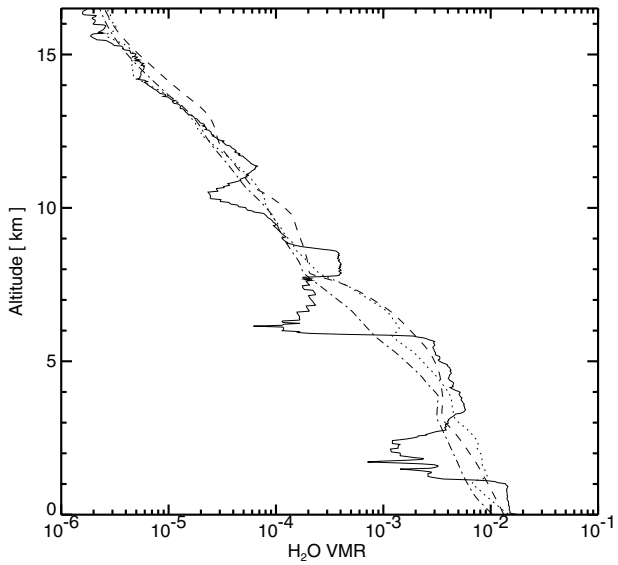

Figure 5. A high-resolution radiosonde VMR profile (solid), and different smoothed profiles all with 4000 m smoothing height. The smoothed profiles were produced using VMR (dashed), log(VMR) (dash-dotted), and RH (dotted) smoothing. This is the profile that showed the largest difference in OLR for the different smoothing methods.

In order to check whether these randomly sampled 50 profiles can represent the variability of each class, we randomly sampled the 150 TRO profiles into 3 groups of 50 profiles each, calculated OLR, and then analyzed the mean and the variability of OLR for each group. The values are given in Table 2 (TS1, TS2, and TS3). The groups show different values for the mean state; there is about 8 W m^{-2} difference between TS1 and

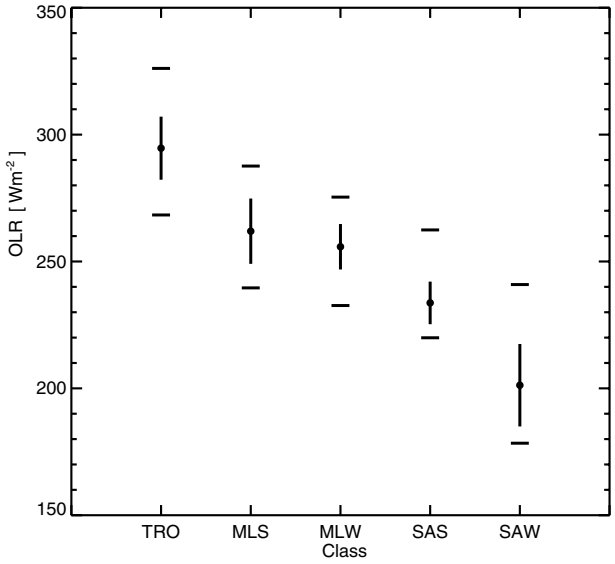

Figure 6. The statistics of OLR for the different radiosonde classes. Dots with vertical error bars mark the mean $\overline{\text{OLR}}$ and standard deviation σ_{OLR}, and the horizontal bars mark the maximum and minimum. The x-axis shows the different climatological classes from tropical (TRO) to subarctic winter (SAW).

TABLE 2. THE STATISTICS (MEAN, STANDARD DEVIATION, MINIMUM AND MAXIMUM) OF OLR (W m^{-2}) AT 100 hPa FOR THE DIFFERENT RADIOSONDE CLASSES

Class	$\overline{\text{OLR}}$	σ_{OLR}	min(OLR)	max(OLR)
TS1	287.81	11.86	266.95	319.49
TS2	293.84	12.02	268.34	320.55
TS3	295.49	11.38	268.36	318.69
TRO	294.66	12.43	268.33	326.10
MLS	261.94	12.87	239.59	287.62
MLW	255.81	8.96	232.65	275.38
SAS	233.68	8.39	219.94	262.44
SAW	201.24	16.25	178.38	240.91

The sample size is 50 randomly selected profiles for each class, as described in section 2(b).

TS2. It is interesting to note that the standard deviations among the groups do not differ significantly; the difference is less than 1 W m^{-2}. This gives us the confidence that the randomly sampled profiles can be used for analysing the OLR variability even though they cannot represent the mean of each climate class.

As shown by Allan *et al.* (1999) and BEB, clear-sky OLR is sensitive to both temperature and humidity changes. It is therefore interesting to assess which factor is dominating this OLR variability. Because temperature is highly correlated throughout the troposphere, it makes sense to take the surface temperature as a proxy for tropospheric temperature. To verify that the surface temperature is a good proxy for the tropospheric temperature, we calculated a quantity called mean tropospheric temperature (MTT), which is defined as the mean temperature between surface and 200 hPa, and then calculated its correlation with surface temperature. We found that the correlation is 0.95. Figure 7 shows a scatter plot of OLR versus surface temperature for the AWI

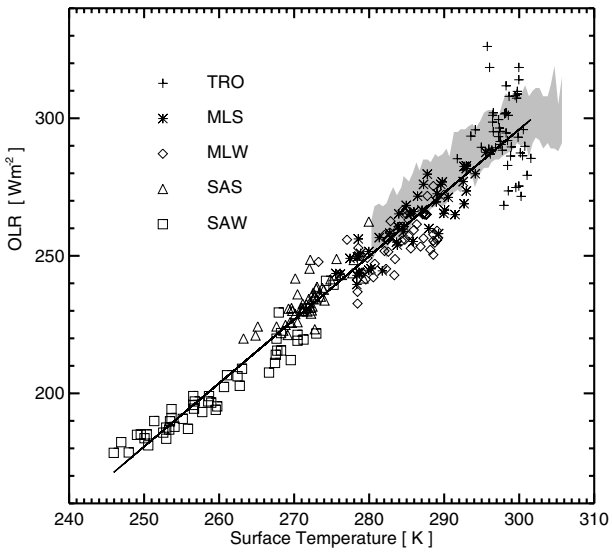

Figure 7. Calculated OLR at 100 hPa as a function of surface temperature for the five different radiosonde classes. The solid line is a linear fit to the data from all five classes. The grey shaded area shows the one standard deviation variability of clear-sky CERES/TRMM data taken from Inamdar *et al.* (2004). Unfortunately, these data are only available for surface temperatures above 280 K.

radiosonde data and the calculated OLR. Different symbols mark the different climatological classes.

To check the consistency of our calculations, we can use data from the Clouds and the Earth's Radiant Energy System (CERES) instrument on board the Tropical Rainfall Measuring Mission (TRMM) satellite. The grey shaded area in Fig. 7 shows the $\pm$ one standard deviation variability of CERES/TRMM clear-sky OLR data from Inamdar *et al.* (2004). Because the TRMM orbit does not cover high latitudes, CERES/TRMM data are not available for surface temperatures below 280 K. Our simulated OLR values are consistent with the CERES data, although at the lower end of the CERES variability.

It should be noted that this consistency check is not a validation of our calculated OLR. It is impractical to validate the calculated OLR using the CERES data for the following reasons:

(a) CERES measurements are only for a shorter time period, from January to December 1998. A validation procedure should be made using collocated (in space and time) atmospheric profiles. The atmospheric profiles used in this study are not collocated with CERES data in either time or space.

(b) The definition of clear-sky OLR in our case and satellite-estimated OLR are different as discussed in the introduction. Due to cloud filtering, CERES data do not sample the most humid conditions which are associated with the lowest OLR values. For example, the CERES data do not show the low values of clear-sky OLR at $\sim$300 K present in the radiosonde calculations which presumably sample moist, cloudy conditions.

(c) We calculate OLR at 100 hPa whereas CERES measures the top of the atmosphere OLR.

The comparison in Fig. 7 is thus not intended as a validation, but only as a rough consistency check. Considering the above limitations, the agreement can be considered

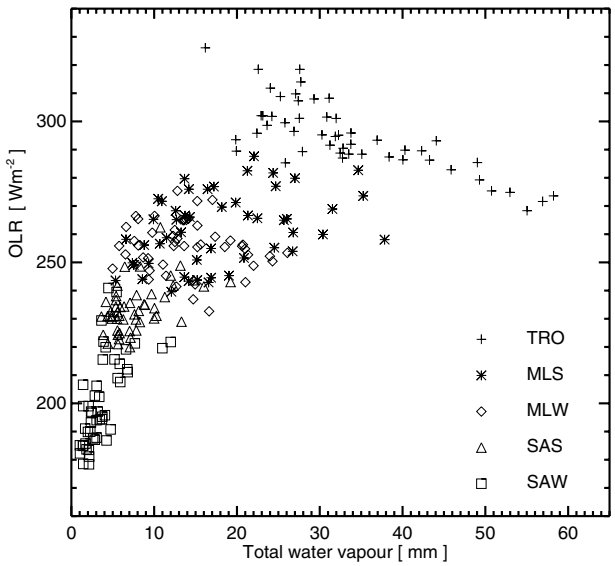

Figure 8. Calculated OLR as a function of total column water vapour for the five radiosonde classes. Only the TRO class shows the expected negative humidity signal; for the other classes it is outweighed by the stronger positive temperature signal.

very good. A possibility for a true validation would be to use data from the ERBE experiment, but this is beyond the scope of this study.

Figure 7 shows that there is generally a very good correlation between surface temperature and OLR. The parameters obtained by a linear fit are

$$\mathrm{OLR_{Tfit}} = 2.306\, T_{\mathrm{surface}} - 395.984. \tag{1}$$

The standard deviation of $\mathrm{OLR_{Tcorr}} = \mathrm{OLR} - \mathrm{OLR_{Tfit}}$ is 8.5 W m^{-2}. The only notable exception is the TRO class, for which there is considerably more scatter than for the other classes. The reason for this can be understood from Fig. 8, which displays OLR as a function of total column water vapour (TWV). It shows that for the TRO class the variability in OLR is dominated by humidity changes, not temperature changes. Only for the TRO class does OLR decrease with increasing humidity, showing the water vapour signal. For the other classes OLR increases with increasing TWV, which means that one sees here again the temperature signal, not the humidity signal (higher TWV usually implies higher tropospheric temperature). This confirms the result that Allan *et al.* (1999) derived from OLR simulations based on ECMWF 45-year re-analysis (ERA-40) data.

The different behaviour in the tropics is simply because surface temperature changes there are not as large. Or, put differently, the sensitivity to humidity changes is also present for the other classes, but masked by the large temperature variability. This can be demonstrated by plotting $\mathrm{OLR_{Tcorr}}$ versus Total Tropospheric Humidity (TTH, defined here as the average RH between the surface and 200 hPa), as shown in Fig. 9 for the TRO and SAW class. It should be noted that tropospheric temperature and TTH are not correlated; the correlation is only -0.22 between MTT and TTH or -0.17 between surface temperature and TTH. Thus, surface temperature and TTH can be considered to be independent variables and the moisture variability will not contain the influence of temperature. This would not have been true if we had taken TWV as a proxy for tropospheric humidity because tropospheric temperature and TWV are highly

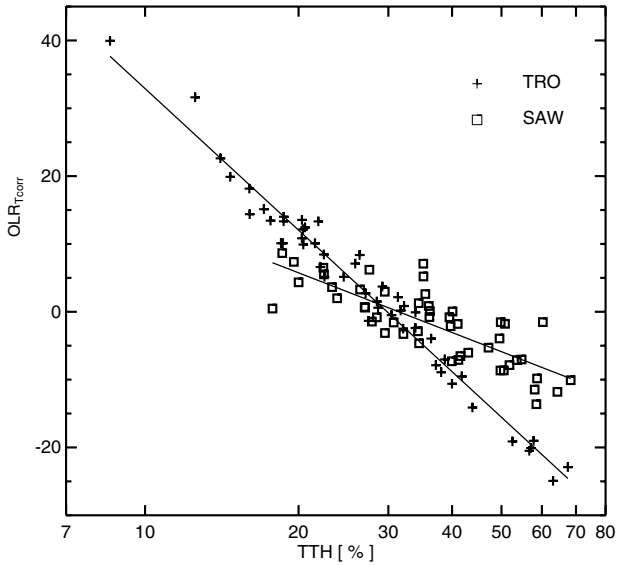

Figure 9. Temperature-corrected OLR_{Tcorr} versus Total Tropospheric Humidity (TTH). Only the TRO and SAW classes are shown to avoid clutter.

TABLE 3. FIT PARAMETERS AND RESIDUAL VARIABILITY (ALL W m^{-2}) FOR EQ. (3).

Class	a	b	σ_{res}
TRO	−30.108	−293.752	2.368
MLS	−14.800	−343.690	2.945
MLW	−17.915	−336.553	2.294
SAS	−12.216	−348.307	3.352
SAW	−12.691	−352.221	3.261

Parameter a is for TTH in fractional RH, not in %RH.

correlated (0.83). The figure confirms that, for a given surface temperature, the OLR variability is indeed to a large extent due to RH variations. Moreover, there is a simple exponential relationship between TTH and OLR_{Tcorr} (note that TTH is plotted on a logarithmic scale). A fit to these data was made, according to

$$\Delta OLR_{Hfit} = a \ln(TTH) + B. \quad (2)$$

The two fit examples show that this relationship is fulfilled quite well. The other classes show a similarly good quality of fit, but were omitted for clarity. Equations (1) and (2) can be combined into one to predict clear-sky OLR based on surface temperature and TTH as

$$OLR = 2.306\, T_{surface} + a \ln(TTH) + b. \quad (3)$$

Table 3 summarizes for all classes the fit parameters a and b, as well as the residual variability, defined as the standard deviation of the difference between the data and the fitted OLR from Eq. (3). The residual variability is only 2.3–3.4 W m^{-2}, depending on the radiosonde class.

(*b*) *Impact of vertical structure*

The residual variability after surface temperature and TTH correction must be due to the vertical distribution of temperature and humidity. This brings up the problem that

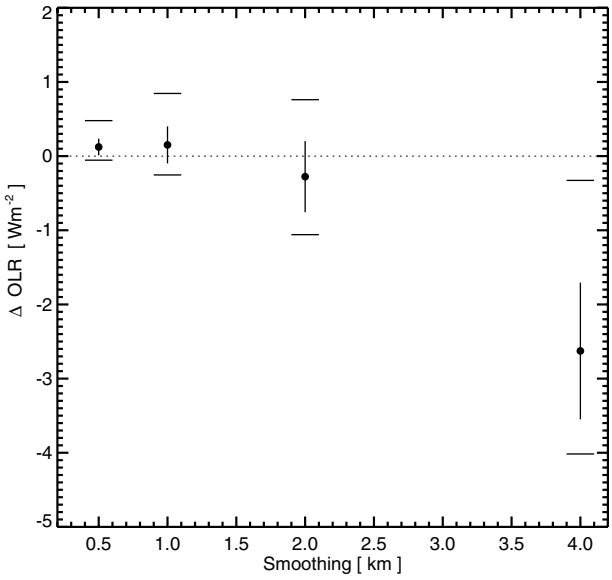

Figure 10. The statistics of the deviation of OLR for smoothed profiles from the high-resolution reference: the mean difference and its standard deviation, together with maximum and minimum values. This is for the TRO class with VMR smoothing.

vertical structure is measured only with a coarse resolution by typical remote-sensing instruments. To assess this, simulations with smoothed versions of the radiosonde data were carried out.

Figure 10 shows for the TRO class the statistics of the change in OLR if the humidity profiles are smoothed in VMR with different smoothing heights. The mean difference for a 4 km smoothing of the TRO class is approximately 2.6 W m^{-2}. Thus, VMR smoothing leads to a significant bias in OLR for smoothing heights above 2 km (compare the number to the 1.6–3.0 W m^{-2} for CO_2 doubling). Limb-sounding instruments, for which the retrieval should do something close to a VMR smoothing, typically have smoothing heights of approximately 2.5 km or slightly better.

Downward-looking passive instruments like the High Resolution Infrared Radiation Sounder (HIRS, Smith *et al.* 1979) or the Advanced Microwave Sounding Unit (AMSU, Saunders *et al.* 1995) have an intrinsic smoothing height as large as 4 km. However, these instruments are in good approximation sensitive to vertically averaged RH, as shown for example by Soden and Bretherton (1996) for HIRS and by Buehler and John (2005) for AMSU, so that RH smoothing is more appropriate than VMR smoothing. For RH smoothing there is practically no bias, as shown by Fig. 11, which compares the different investigated smoothing methods for 4 km smoothing altitude.

Of all investigated smoothing methods, RH smoothing and VMR_c smoothing are the methods that introduce the smallest bias. The conclusion for RH smoothing holds for all investigated atmospheric classes, as shown by Fig. 12. Thus, OLR calculated from measurements of sensors with such coarse vertical resolutions can indeed have the correct mean values. However, it should not be forgotten that the deviations for individual profiles can be quite high; the standard deviation for the TRO case with 4 km smoothing height is 1 W m^{-2}.

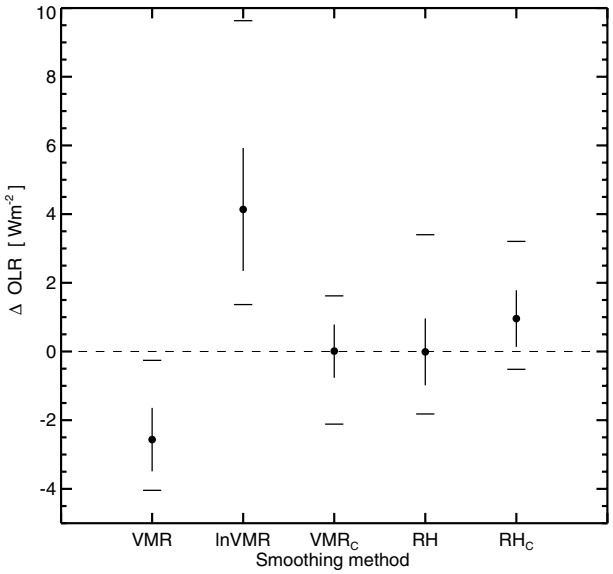

Figure 11. The impact of different smoothing methods on OLR for the TRO class for smoothing height 4 km: mean, standard deviation, and maximum and minimum values of the deviation, as in Fig. 10.

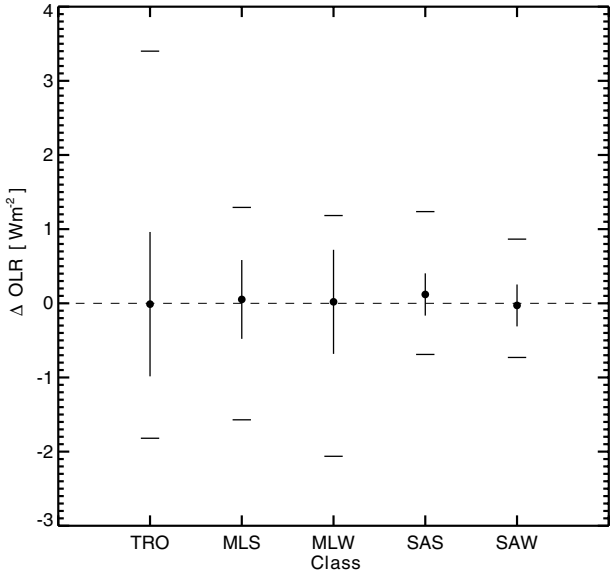

Figure 12. Effect of RH smoothing with 4 km smoothing height for all atmospheric classes: mean, standard deviation, and maximum and minimum values of the deviation, as in Figs. 10 and 11.

4. SUMMARY AND CONCLUSIONS

A high-frequency-resolution radiative transfer model with state-of-the-art continuum parametrizations was used to simulate clear-sky outgoing long-wave radiation (OLR) fluxes for a radiosonde dataset with near-global latitudinal coverage, but limited

to ocean areas. The values obtained were found to be in reasonable agreement with CERES/TRMM data. These simulations were used to study the mean and in particular the variability of OLR over ocean for different climate zones and seasons. The variability was interpreted in a quantitative way by relating it to the variability of temperature and humidity.

The study used only 50 radiosonde profiles for each climate zone and season, taken during voyages between 1982 and 2003. This sample is too small to estimate correct global mean values. However, by selecting different sub-samples of the available data, it was shown that the variability estimates are robust, in spite of the small sample size, even though the mean values are not.

The overall variability in clear-sky OLR is approximately 33 W m^{-2}, estimated by the standard deviation of all OLR values calculated from AWI radiosondes. This large variability can be explained to a large extent by variations in the effective tropospheric temperature, or in the surface temperature as a proxy. That component of the variability can be removed by making a linear fit of OLR versus surface temperature. The remaining variability is approximately 8.5 W m^{-2}. Of this remaining variability, a significant part can be explained by variations in the Total Tropospheric Humidity (TTH). Making a linear fit of the temperature-independent OLR variations against the logarithm of TTH reduces the remaining variability to only approximately 3 W m^{-2}.

This remaining variability must be due to vertical structure. It was shown that humidity structures on a vertical scale smaller than 4 km contribute a variability of approximately 1 W m^{-2}, but no significant bias if the smoothing is done in the right way. The right way to smooth is in RH; if the smoothing is done in VMR for example, it leads to a substantial bias. This result means that measurements from sensors with coarse vertical resolution may be used to predict OLR with the correct mean values, but will not be able to fully reproduce the variability due to vertical structures, as almost half of that can come from structures on a scale smaller than 4 km. This calls for sensors that can sound the troposphere, including the upper troposphere, with good vertical resolution. Such sensors could use the LEO–LEO radio occultation technique (Eriksson *et al.* 2003) as with the proposed Atmosphere and Climate Explorer (ACE+) instrument (Battrick 2004), the passive microwave limb-sounding technique as with the MLS instrument on the EOS-Aura satellite (Waters *et al.* 1999), or the high-spectral-resolution instruments such as the Atmospheric Infrared Sounder (AIRS) and Infrared Atmospheric Sounding Interferometer (IASI).

Another big issue is the absolute accuracy of the sensor for humidity measurements, because there are large discrepancies in the upper tropospheric humidity (UTH) measured by the different sensors currently in use. For example, according to Soden *et al.* (2004), the relative difference in UTH between Väisälä radiosondes and the HIRS satellite sensor is approximately 40% (the difference in UTH between Raman lidar and HIRS measurements is approximately 10%). If we assume a 40% uncertainty in UTH, it may introduce a bias in clear-sky OLR of approximately 3.8 W m^{-2} for the MLS scenario, a number derived by sensitivity calculations similar to those presented in BEB. This is a significant uncertainty; to put it into perspective, we note that the forcing associated with doubling CO_2 is only 1.6–3.0 W m^{-2} according to BEB. Even a modest 10% uncertainty in UTH still leads to a clear-sky OLR bias of 1 W m^{-2}.

The large uncertainty in UTH and associated uncertainty in OLR is a strong argument in favour of implementing a system to globally measure UTH with high absolute accuracy. This could for example be achieved by a satellite humidity mission, using the self-calibrating LEO–LEO radio occultation technique (Battrick 2004).

ACKNOWLEDGEMENTS

Thanks go to P. Mills, Institute of Environmental Physics University of Bremen, for his help in processing the radiosonde data, and to Jonathan P. Taylor, Met Office (UK), for a discussion about the CERES data. Thanks also go to Atmospheric and Environmental Research Inc., in particular T. Clough and E. Mlawer, for making the latest continuum models publicly available at http://www.rtweb.aer.com/continuum_frame.html. Furthermore, thanks go to the ARTS radiative transfer community, many of whom have indirectly contributed by implementing features to the ARTS model. This study was funded by the German Federal Ministry of Education and Research (BMBF), within the AFO2000 project UTH-MOS, grant 07ATC04, and by the ESA project ACECLIM, ESTEC Contract No. 17479/03/NL/FF. It is a contribution to COST Action 723 'Data Exploitation and Modeling for the Upper Troposphere and Lower Stratosphere'.

REFERENCES

Allan, R. P., Shine, K. P., Slingo, A. and Pamment, J. A. 1999 The dependence of clear-sky outgoing long-wave radiation on surface temperature and relative humidity. *Q. J. R. Meteorol. Soc.*, **125**, 2103–2126

Anderson, G. P., Clough, S. A., Kneizys, F. X., Chetwynd, J. H. and Shettle, E. P. 1986 'AFGL atmospheric constituent profiles (0–120 km)'. Tech. Report TR-86-0110, AFGL, Lexington, Mass., USA

Battrick, B. 2004 'ACE+ Atmosphere and Climate Explorer, Report for Mission Selection'. ESA report SP-1279(4), European Space Agency, Noordwijk, The Netherlands

Buehler, S. A. and John, V. O. 2005 A simple method to relate microwave radiances to upper tropospheric humidity. *J. Geophys. Res.*, **110,** D02110, doi: 10.1029/2004JD005111

Buehler, S. A., Eriksson, P., Kuhn, T., von Engeln, A. and Verdes, C. 2005 ARTS, the atmospheric radiative transfer simulator. *J. Quant. Spectrosc. Radiat. Transfer*, **91**(1)**,** 65–93

Buehler, S. A., von Engeln, A., Brocard, E., John, V. O., Kuhn, T. and Eriksson, P. 2006 Recent developments in the line-by-line modeling of outgoing longwave radiation. *J. Quant. Spectrosc. Radiat. Transfer*, **98**(3)**,** 446–457

Chevallier, F. 2001 'Sampled databases of 60-level atmospheric profiles from the ECMWF analysis'. EUMETSAT/ECMWF SAF program research report No. 4, available at: http://www.met-office.gov.uk/research/interproj/nwpsaf/rtm/profiles.pdf

Clough, S. A. and Iacono, M. J. 1995 Line-by-line calculation of atmospheric fluxes and cooling rates. 2: Application to carbon dioxide, ozone, methane, nitrous oxide and the halocarbons. *J. Geophys. Res.*, **100,** D8, 16519–16535

Clough, S. A., Iacono, M. J. and Moncet, J.-L. 1992 Line-by-line calculations of atmospheric fluxes and cooling rates: Application to water vapor. *J. Geophys. Res.*, **97,** D14, 15761–15785

Clough, S. A., Shephard, M. W., Mlawer, E., Delamere, J. S., Iacono, M., Cady-Pereira, K., Boukabara, S. and Brown, P. 2005 Atmospheric radiative transfer modeling: a summary of the AER codes. *J. Quant. Spectrosc. Radiat. Transfer*, **91,** 233–244

Colman, R. A. 2001 On the vertical extent of atmospheric feedbacks. *Clim. Dyn.*, **17,** 391–405

Eriksson, P., Jimenez, C., Murtagh, D., Elgered, G., Kuhn, T. and Buehler, S. 2003 Measurement of tropospheric/stratospheric transmission at 10–35 GHz for H_2O retrieval in low earth orbiting satellite links. *Radio Sci.*, **38**(4)**,** 8069, doi: 10.1029/2002RS002638

Harries, J. E. 1996 The greenhouse earth: A view from space. *Q. J. R. Meteorol. Soc.*, **122**, 799–818

1997 Atmospheric radiation and atmospheric humidity. *Q. J. R. Meteorol. Soc.*, **123,** 2173–2186

Held, I. M. and Soden, B. J. 2000 Water vapor feedback and global warming. *Ann. Rev. Energy Environ.*, **25,** 441–475

Inamdar, A. K., Ramanathan, V. and Loeb, N. G. 2004 Satellite observations of the water vapor greenhouse effect and column longwave cooling rates: Relative roles of the continuum and vibration-rotation to pure rotation bands. *J. Geophys. Res.*, **109,** D06104, doi: 10.1029/2003JD003980

Kiehl, J. T. and Trenberth, K. E. 1997 Earth's annual global mean energy budget. *Bull. Am. Meteorol. Soc.*, **78**(2)**,** 197–208

Koenig-Langlo, G. and Marx, B. 1997 The meteorological information system at the Alfred Wegener Institute. Pp. 11–125 in *Climate and environmental database systems*, Eds. M. Lautenschlager and M. Reinke. Kluwer Academic

Lindzen, R. S. 1990 Some coolness concerning global warming. *Bull. Am. Meteorol. Soc.*, **71,** 288–299

Newman, S. M., Smith, J. A., Glew, M. D., Rogers, S. M. and Taylor, J. P. 2005 Temperature and salinity dependence of sea surface emissivity in the thermal infrared. *Q. J. R. Meteorol. Soc.*, **131,** 2539–2557

Rothman, L. S., Barbe, A., Benner, D. C., Brown, L. R., Camy-Peyret, C., Carleer, M. R., Chance, K., Clerbaux, C., Dana, V., Devi, V. M., Fayt, A., Flaud, J.-M., Gamache, R. R., Goldman, A., Jacquemart, D., Jucks, K. W., Lafferty, W. J., Mandin, J.-Y., Massie, S. T., Nemtchinov, V., Newnham, D. A., Perrin, A., Rinsland, C. P., Schroeder, J., Smith, K. M., Smith, M. A. H., Tang, K., Toth, R. A., Auwera, J. V., Varanasi, P. and Yoshino, K. 2003 The HITRAN molecular spectroscopic database: Edition of 2000 including updates of 2001. *J. Quant. Spectrosc. Radiat. Transfer*, **82,** 5–44

Salby, M. L. 1996 *Fundamentals of atmospheric physics*. Vol. 61 of International Geophysics Series, Academic Press

Saunders, R. W., Hewison, T. J., Stringer, S. J. and Atkinson, N. C. 1995 The radiometric characterization of AMSU-B. *IEEE Trans. Microw. Theory*, **43**(4)**,** 760–771

Shine, K. P. and Sinha, A. 1991 Sensitivity of the earth's climate to height-dependent changes in the water vapour mixing ratio. *Nature*, **354,** 382–384

Sinha, A. and Allen, M. R. 1994 Climate sensitivity and tropical moisture distribution. *J. Geophys. Res.*, **99,** D2, 3707–3716

Sinha, A. and Harries, J. E. 1995 Water vapor and greenhouse trapping—the role of far-infrared absorption. *J. Geophys. Res.*, **22,** 2147–2150

Slingo, A., Pamment, J. A. and Webb, M. J. 1998 A 15-year simulation of the clear-sky greenhouse effect using the ECMWF reanalysis: Fluxes and comparisons with ERBE. *J. Climate*, **11,** 690–708

Smith, W. L., Woolf, H. M., Hayden, C. M., Wark, D. Q. and McMillin, L. M. 1979 The TIROS-N operational vertical sounder. *Bull. Am. Meteorol. Soc.*, **60,** 1177–1187

Soden, B. J. and Bretherton, F. P. 1996 Interpretation of TOVS water vapor radiances in terms of layer-average relative humidities: Method and climatology for the upper, middle and lower troposphere. *J. Geophys. Res.*, **101,** D5, 9333–9343

Soden, B. J. and Lanzante, J. R. 1996 An assessment of satellite and radiosonde climatologies of upper tropospheric water vapor. *J. Climate*, **9**(6)**,** 1235–1250

Soden, B. J., Wetherald, R. T., Stenchikov, G. L. and Robock, A. 2002 Global cooling after the eruption of Mount Pinatubo: A test of climate feedback by water vapor. *Science*, **296**, 727–730

Soden, B. J., Turner, D. D., Lesht, B. M. and Miloshevich, L. M. 2004 An analysis of satellite, radiosonde, and lidar observations of upper tropospheric water vapor from the atmospheric radiation measurement program. *J. Geophys. Res.*, **109,** D04105, doi: 10.1029/2003JD003828

von Engeln, A., Brocard, E., Buehler, S. A., Eriksson, P., John, V. O. and Kuhn, T. 2004 'ACE+ climate impact study: Radiation part, final report'. Tech. report, ESTEC Contract No. 17479/03/NL/FF. Available at: http://www.sat.uni-bremen.de/projects/occultation/publications/ACECLIM_Final_Report.pdf

Waters, J. W., Read, W. G., Froidevaux, L., Jarnot, R. F., Cofield, R. E., Flower, D. A., Lau, G. K., Pickett, H. M., Santee, M. L., Wu, D. L., Boyles, M. A., Burke, J. R., Lay, R. R., Loo, M. S., Livesey, N. J., Lungu, T. A., Manney, G. L., Nakamura, L. L., Perun, V. S., Ridenoure, B. P., Shippony, Z., Siegel, P. H., Thurstans, R. P., Harwood, R. S., Pumphrey, H. C. and Filipiak, M. J. 1999 The UARS and EOS microwave limb sounder experiments. *J. Atmos. Sci.*, **56,** 194–218